Supplement of Geosci. Model Dev., 19, 2881–2901, 2026
https://doi.org/10.5194/gmd-19-2881-2026-supplement

Geoscientific Model Development
Open Access
EGU

Supplement of

Towards improved Euro-Mediterranean discharge simulations in regional coupled climate models: a comparative assessment of hydrologic performance

Mohamed Hamitouche et al.

Correspondence to: Mohamed Hamitouche (mohamed.hamitouche@iusspavia.it)

Text S1:

To investigate the influence of meteorological forcing errors, we assessed the performance of WRF precipitation input by calculating the mean daily percent bias relative to EOBS precipitation data for each basin (Figure S7).

The results reveal a mixed pattern of biases, ranging from slight underestimations, such as in the Danube (-1.2%) and Po (1.7%) basins, to substantial overestimations, as seen in the Adige (32.5%) and Kopru (27.7%) basins. Notably, the Tiber basin exhibits a significant underestimation of -27.3%. These findings highlight the variability in precipitation input accuracy across basins, which can directly affect streamflow simulation. Addressing these biases is crucial, especially in basins like the Adige and Tiber, where large deviations could propagate errors through hydrological models, underscoring the need for bias correction and refinement of precipitation datasets.

Text S2:

The calibrated parameters and their respective values for each basin are presented in Table S4. These parameters influence several key physical processes that control the hydrological response. Infiltration is regulated by the parameters bexp, smcmax, dksat, and refkdt, where higher values of these parameters generally lead to increased infiltration. Soil evaporation, on the other hand, is primarily governed by rsurfexp and smcmax, with elevated values of both promoting higher soil evaporation rates.

Aquifer recharge is strongly affected by the slope parameter. Lower values of slope reduce the transfer of water from the soil column to the groundwater reservoir, thereby decreasing aquifer recharge. Similarly, baseflow is influenced by zmax, expon, and coeff. High values of zmax tend to suppress baseflow contributions to river discharge, while higher values of expon and coeff increase it.

Transpiration processes are controlled by the parameters cwpvt, mp, vcmx25, and hvt. A decrease in cwpvt leads to higher transpiration rates, whereas lower values of mp, vcmx25, and hvt result in reduced transpiration. Overland flow routing, which is affected by retdeprtfac and ovroughrtfac, decreases with higher values of these parameters. Subsurface flow is governed by lksatfac, where an increase in its value enhances subsurface water movement.

The calibration process revealed some notable overall trends across all basins. There was a consistent increase in refkdt, which controls runoff partitioning and results in a higher proportion of subsurface runoff compared to surface runoff. Additionally, the slope parameter consistently decreased, reducing deep drainage from the soil column to the groundwater reservoir. The zmax parameter showed a general increase across most basins, except for Göksu, leading to reduced baseflow contributions to river discharge.

While these three parameters exhibited relatively uniform behaviour across all basins, others displayed more variable trends. For instance, parameters such as bexp, smcmax, dksat, and rsurfexp showed both increases and decreases depending on the basin, reflecting local hydrological conditions.

This variability underscores the complexity of the calibration process. The interplay between parameters often determines the final hydrological outcome, as the effect of one parameter can be moderated or even compensated by another influencing the

same physical process. In some cases, one parameter may dominate over others, masking their effects. These findings highlight the importance of considering the combined influence of multiple parameters to ensure accurate and balanced calibration for hydrological modelling.

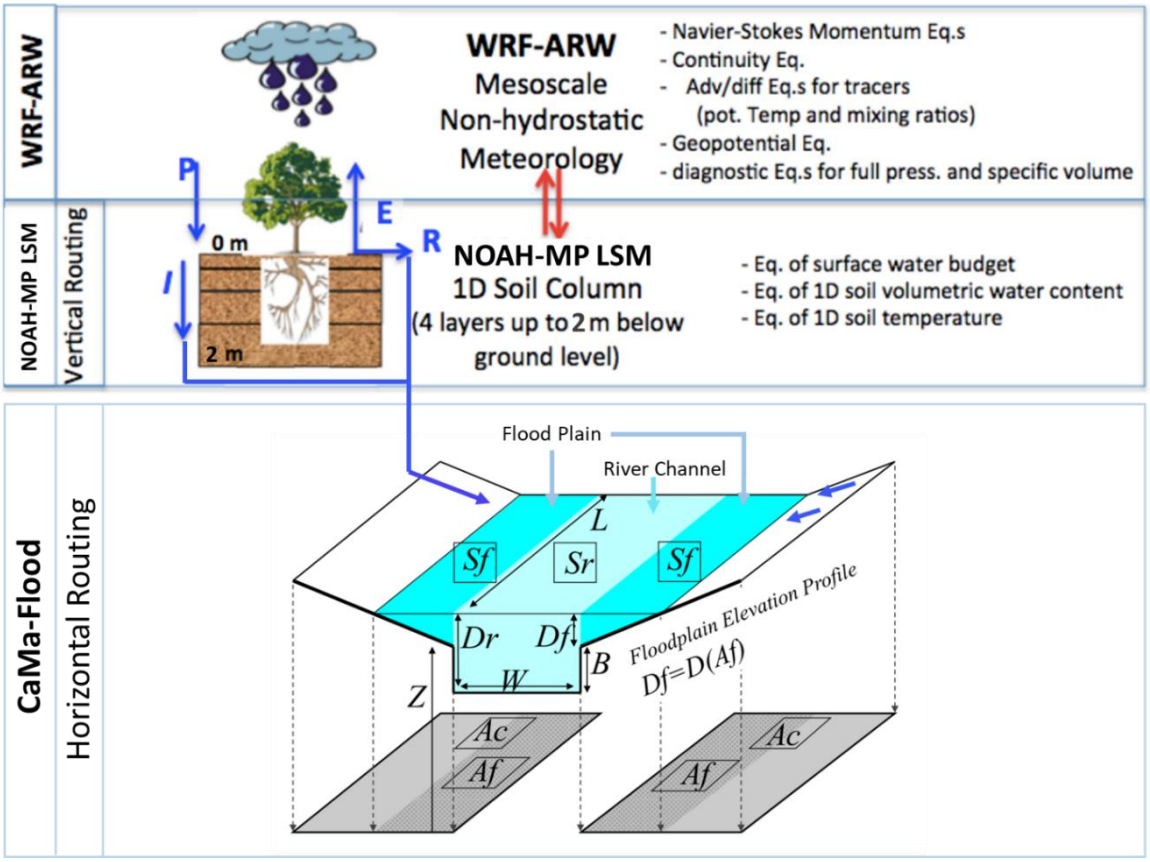

Figure S1: Flowchart of the offline coupling between WRF and CaMa-Flood models (adapted from Yamazaki et al. (2011) and https://www.gewexevents.org/wp-content/uploads/Rasmussen_WRFHydro_USRHP2016.pdf

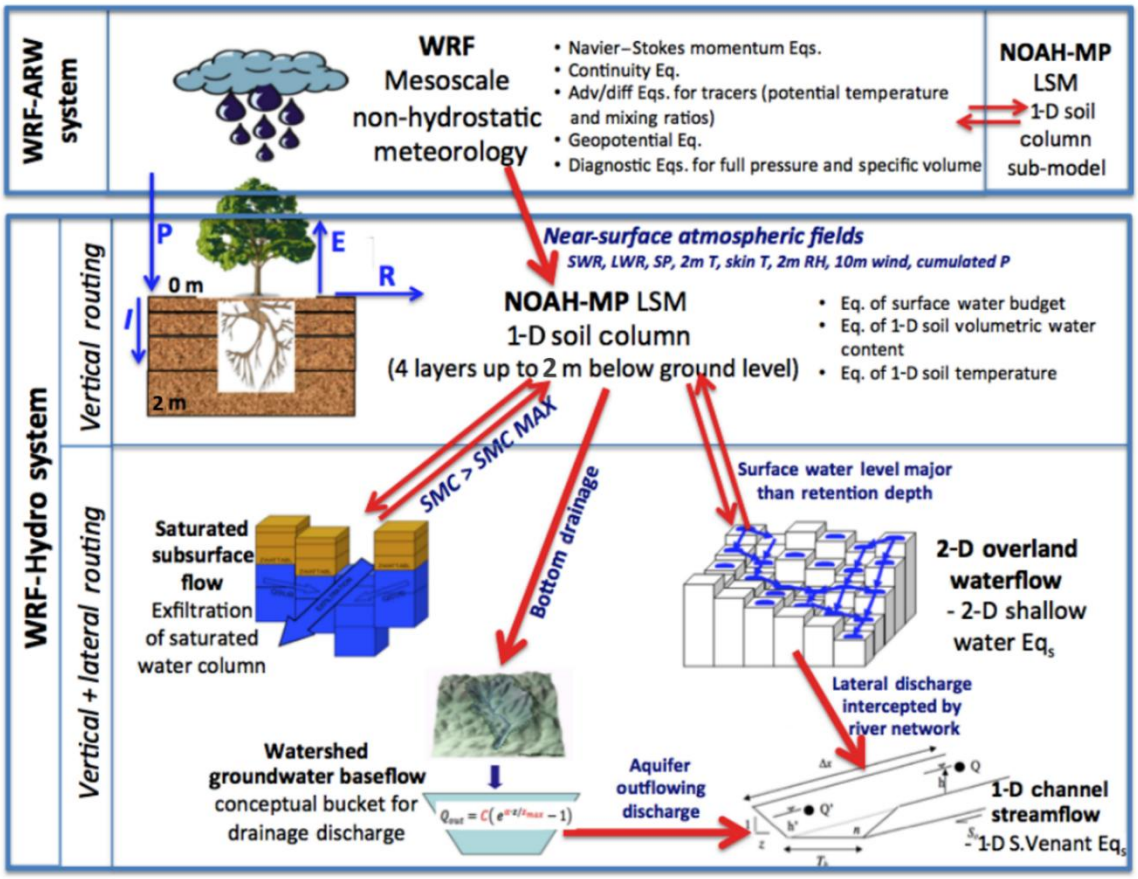

Figure S2: The schematic structure of the offline coupled WRF/WRF-Hydro model (adapted from Verri et al. (2017)).

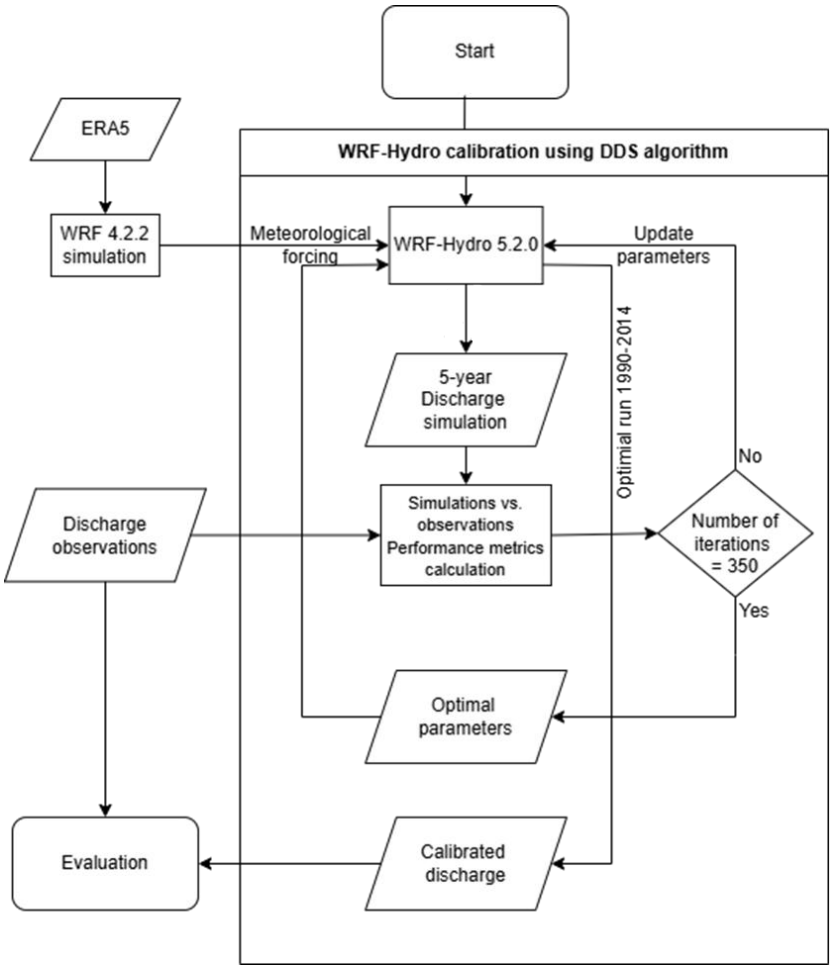

Figure S3: WRF-Hydro calibration flowchart.

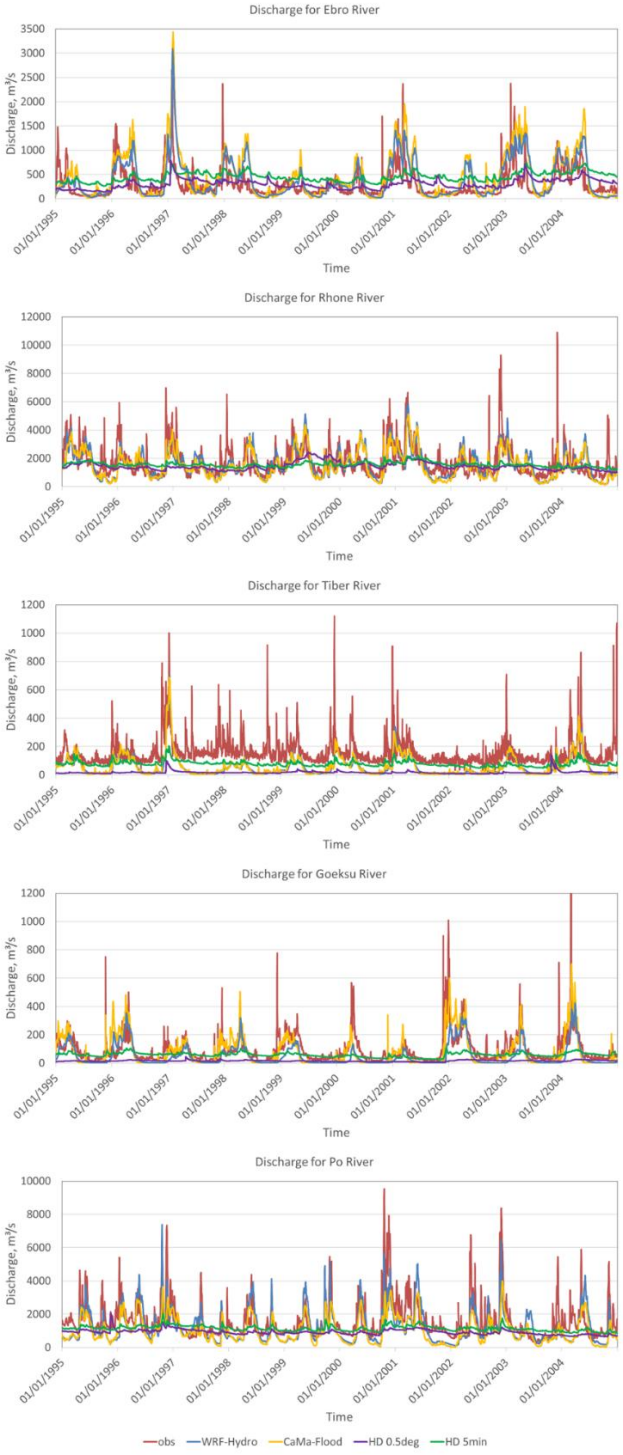

Figure S4: Observed and simulated daily discharge for the Ebro, Rhone, Tiber, Goeksu and Po rivers for common 10 years from 1995 to 2004. Simulations include ENEA-REG–driven WRF-Hydro and CaMa-Flood, as well as the HD model at 0.5-degree and 5-minute spatial resolutions, evaluated near the corresponding gauge stations.

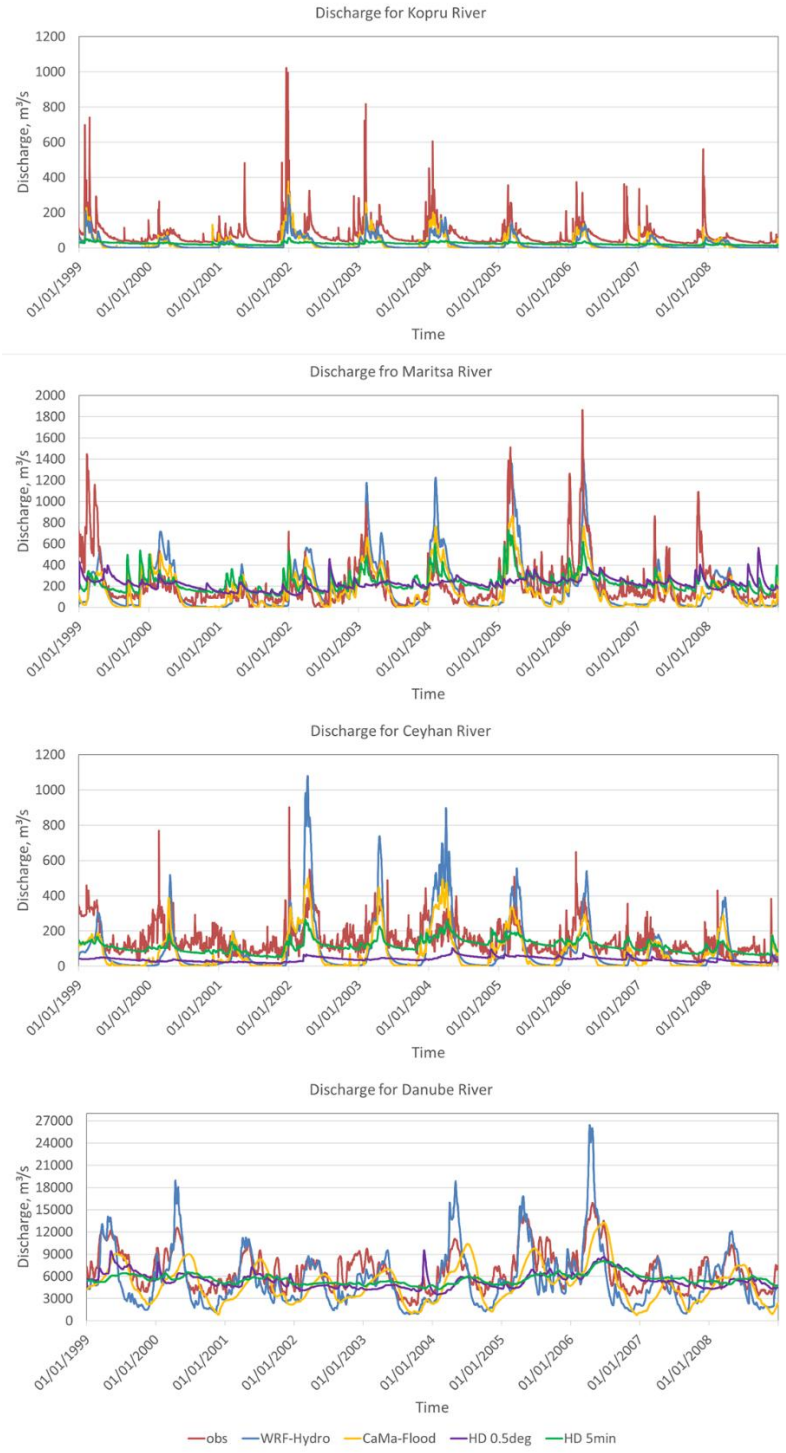

Figure S4 (continuity): Observed and simulated daily discharge for the Kopru, Maritsa, Ceyhan and Danube rivers for common 10 years from 1999 to 2008. Simulations include ENEA-REG–driven WRF-Hydro and CaMa-Flood, as well as the HD model at 0.5-degree and 5-minute spatial resolutions, evaluated near the corresponding gauge stations.

55

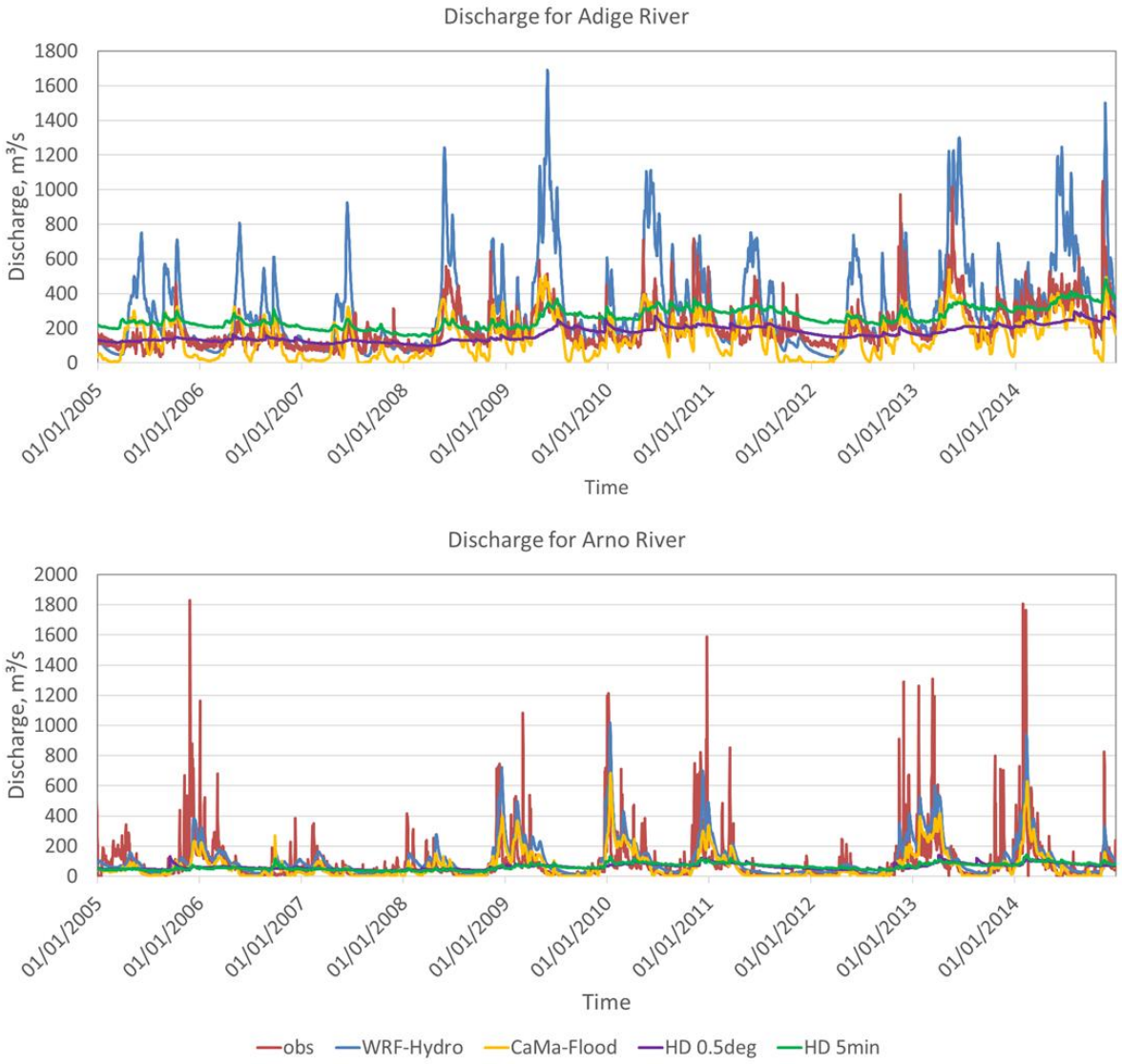

Figure S4 (continuity): Observed and simulated daily discharge for the Adige and Arno rivers for common 10 years from 2005 to 2014. Simulations include ENEA-REG–driven WRF-Hydro and CaMa-Flood, as well as the HD model at 0.5-degree and 5-minute spatial resolutions, evaluated near the corresponding gauge stations.

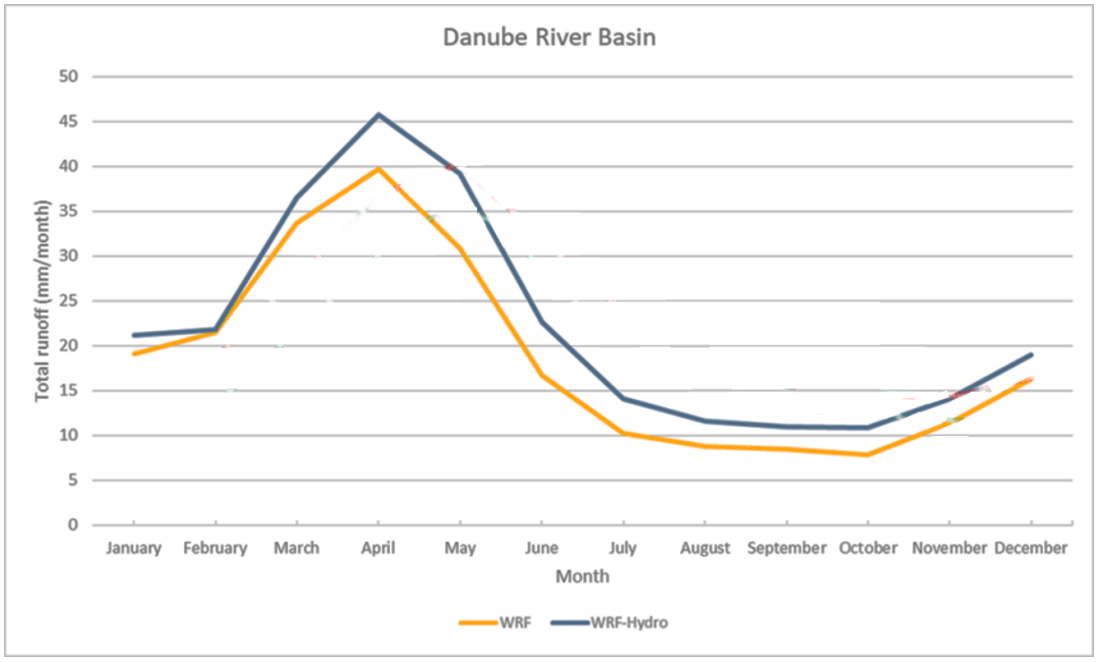

Figure S5: Mean seasonal cycle of runoff (mm) simulated by WRF in ENEA-REG and WRF-Hydro.

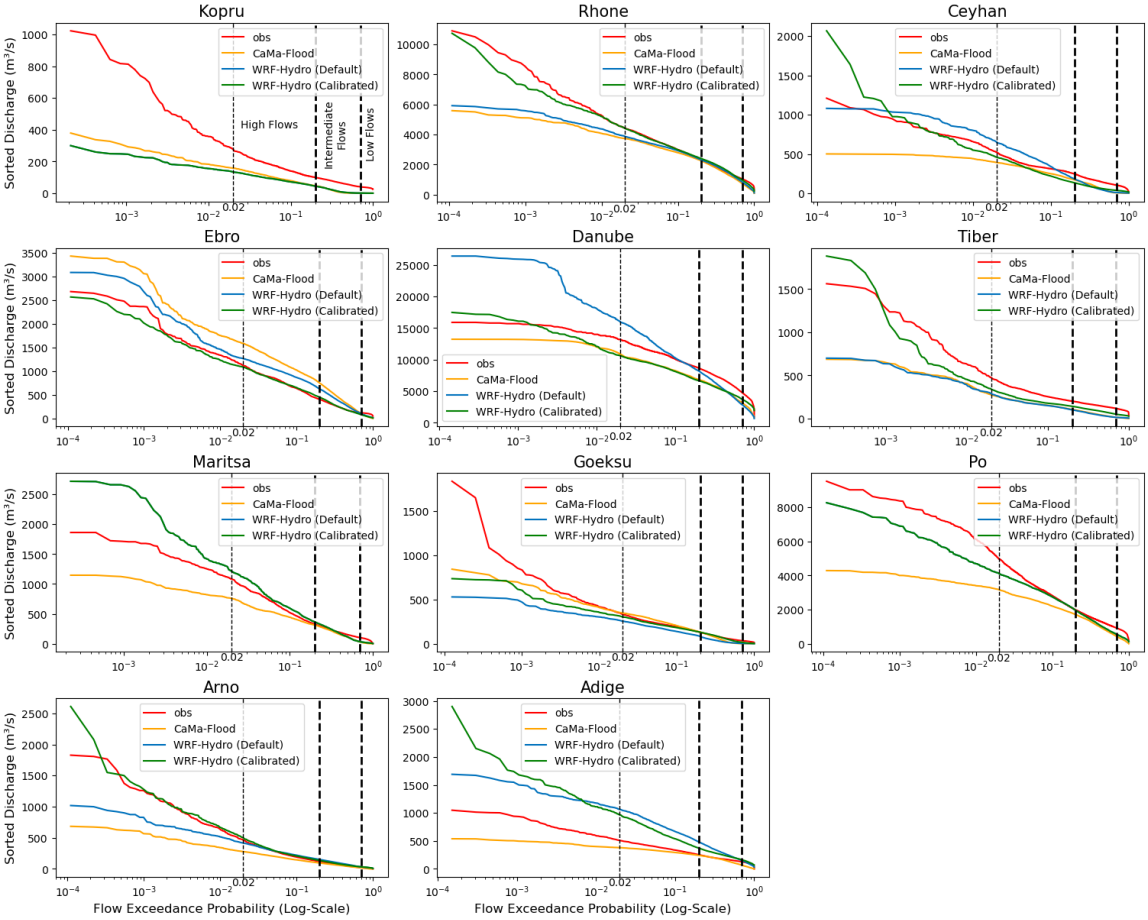

Figure S6: Flow duration curves for each model experiment and basin, with log-scale exceedance probabilities to better visualize the high flows.

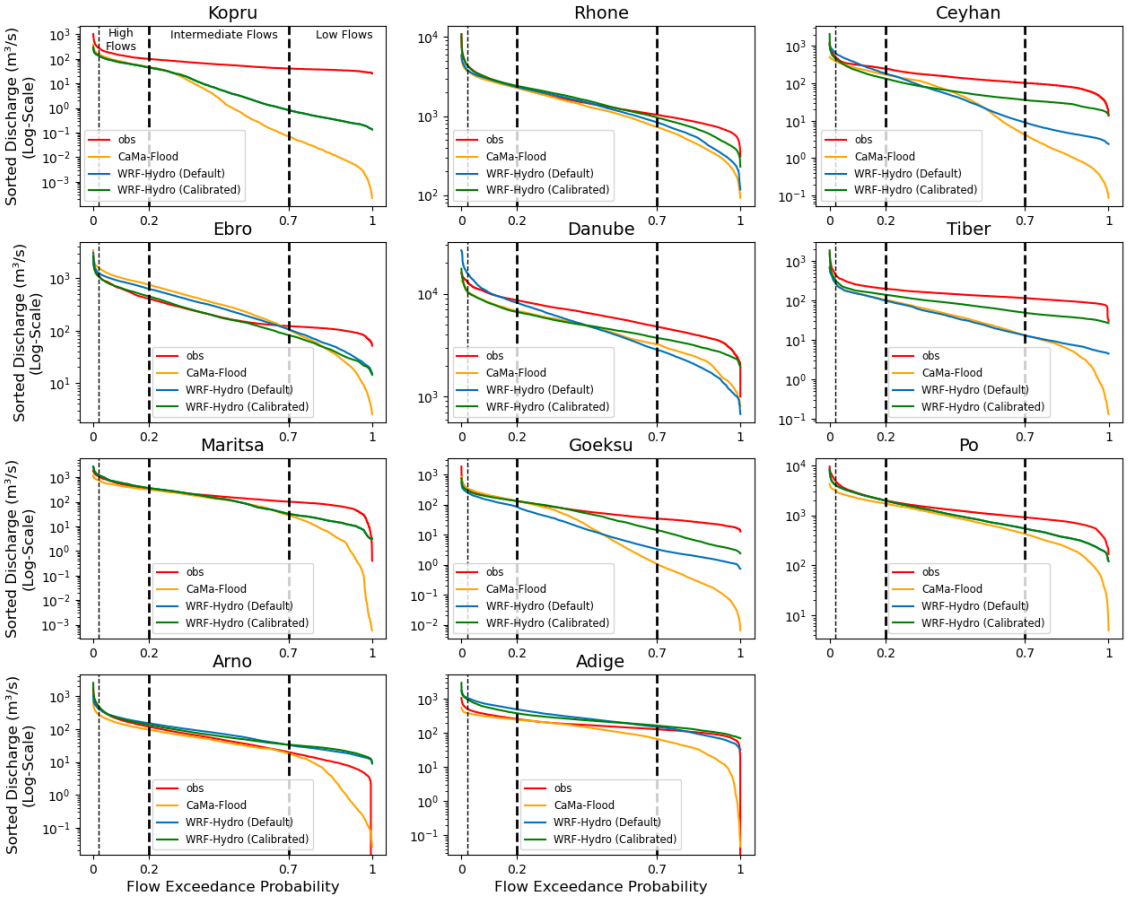

Figure S7: Flow duration curves for each model experiment and basin, with log-scale discharge values to better visualize the low flows.

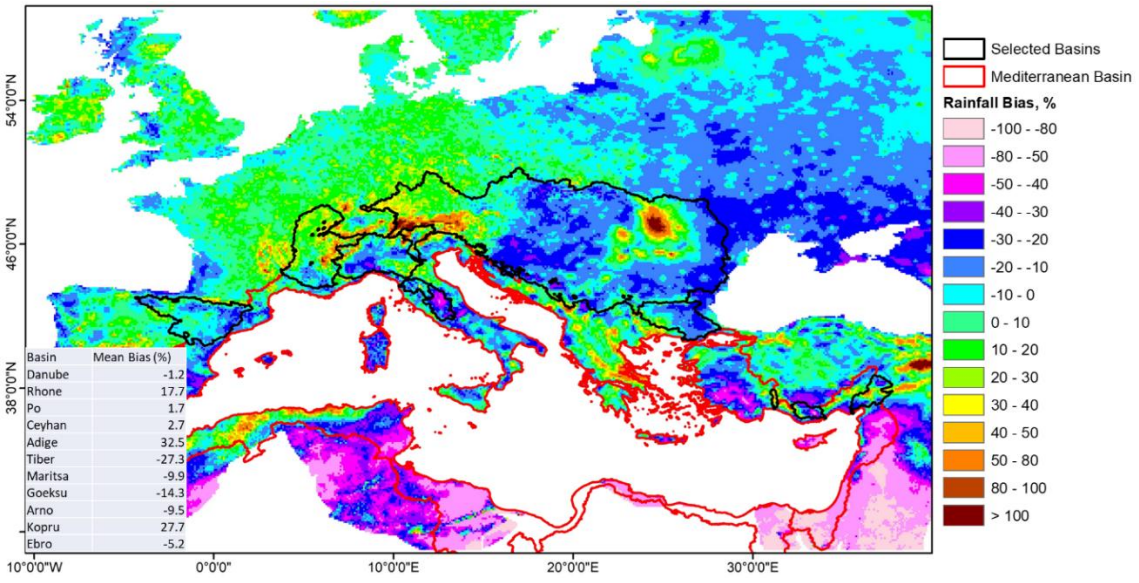

Figure S8: Distribution of the mean daily rainfall percent bias (100 x (WRF-EOBS)/EOBS)

Table S1: The main physical parametrizations used by the atmospheric WRF model.

Atmospheric model	
Model	WRF (v4.2.2)
Domain	Med-CORDEX
Horizontal resolution	12 km
Domain size	480 x 350 cells (lon x lat)
Vertical resolution	50 hybrid levels up to 10 hPa
Physical time step	60 s
Forcing	ERA5
Relaxation zone	10 points with an exponential relaxation
Microphysics	Morrison (two-moment scheme)
Cumulus parametrisation	BMJ
Shortwave radiation	RRTMG
Longwave radiation	RRTMG
Land-surface model	Noah-MP

Table S2: Selected Noah-MP Multiphysics Parameterization Options for Physical Processes.

Noah-MP multiphysics parameterization	
Physical Process	Option
Dynamic vegetation option	LAI from lookup table Maximum vegetation fraction from climatology
Canopy stomatal resistance	Ball-Berry
Soil moisture factor for stomatal resistance	Noah
Runoff	Schaake
Surface layer drag coefficient	M-O
Frozen soil permeability	Niu and Yang (2006)
Super cooled liquid water	Niu and Yang (2006)
Radiative transfer	Two-stream applied to vegetated fraction
Ground snow surface albedo	CLASS
Precipitation partitioning	Jordan (1991)
Lower boundary condition for soil temperature	Original Noah
Snow/soil temperature time scheme	Semi-implicit with FSNO
Glacier treatment	Ice treatment more like original Noah
Surface resistance to evap/sublimation	Snow/non-snow split

Table S3: WRF-Hydro calibration parameters.

Physical Process	Parameter	Description	Units	Default value	Range	Calibration scalar multiplier
Soil	bexp	Pore size distribution index	-	1	0.4–1.9	Yes
	smcmax	Saturation soil moisture content (i.e., porosity)	Volumetric fraction	1	0.8–1.2	Yes
	dksat	Saturated hydraulic conductivity	m/s	1	0.2–10	Yes
	rsurfexp	Exponent in the resistance equation for soil evaporation	-	5	1–6	No
Runoff	refkdt	Surface runoff parameter	-	1	0.1–4	No
	slope	Coefficient to modify the drainage out the bottom of the last soil layer	0–1	0.3	0–1	No
	retdeprtfac	Multiplier on retention depth limit	-	1	0.1–20,000	No
	lksatfac	Multiplier on lateral hydraulic conductivity	-	1000	10–10,000	No
	ovroughrtfac	Multiplier on 2D overland flow roughness factor	-	1	0.01-1	No
Groundwater	zmax	Maximum conceptual nonlinear reservoir depth	mm	50	10–250	No
	expon	Exponent controlling rate of bucket drainage as a function of depth	-	3	1–8	No
	Coeff	controlling rate of bucket drainage as a function of depth	m^3/s	0.001	0.0001-0.1	No
Vegetation	cwpvt	Canopy wind parameter for canopy wind profile formulation	1/m	1	0.5–2	Yes
	vcmx25	Maximum carboxylation at 25°C	$\mu mol/m^2/s$	1	0.6–1.4	Yes

	mp	Slope of Ball-Berry conductance relationship	-	1	0.6–1.4	Yes
	hvt	Canopy height	m	1	0.25-1.5	Yes

Table S4: Summary table of spinu-up and calibrations periods for each river basin

Basin	Spin-up period	Calibration period (including one-year spin-up)
Danube	01/10/1994 – 01/10/1999	01/10/1999 – 01/10/2005
Rhone	01/10/1985 – 01/10/1990	01/10/1990 – 01/10/1996
Po	01/10/2000 – 01/10/2005	01/10/2005 – 01/10/2011
Ceyhan	01/10/1995 – 01/10/2000	01/10/2000 – 01/10/2006
Adige	01/10/2000 – 01/10/2005	01/10/2005 – 01/10/2011
Tiber	01/10/1992 – 01/10/1997	01/10/1997 – 01/10/2003
Maritsa	01/10/1994 – 01/10/1999	01/10/1999 – 01/10/2005
Goeksu	01/10/1995 – 01/10/2000	01/10/2000 – 01/10/2006
Arno	01/10/2000 – 01/10/2005	01/10/2005 – 01/10/2011
Kopru	01/10/1995 – 01/10/2000	01/10/2000 – 01/10/2006
Ebro	01/10/1994 – 01/10/1999	01/10/1999 – 01/10/2005

Table S5: Summary of the performances (KGE, bias, correlation, relative standard deviation, low-flow and high-flow biases) of HD model at 0.5-degree spatial resolution for each river basin, evaluated over the entire 1990-2014 period. No values are reported for the Kopru basin, as its small size relative to the coarse 0.5-degree resolution prevented extraction of a representative discharge time series.

Basin	KGE	Percent bias	Spearman's rho	Relative SD	High-flow Percent Pbias	Low-flow Percent Pbias
Danube	0.15	-21.88	0.35	0.42	-40.62	-12.44
Rhone	-0.05	-20.92	0.31	0.28	-61.07	-18.73
Po	-0.08	-42.61	0.52	0.18	-77.32	-42.33
Ceyhan	-0.36	-75.77	0.30	0.11	-88.31	-63.25
Adige	0.11	-14.57	0.47	0.33	-57.16	-1.36
Tiber	-0.47	-89.30	0.40	0.10	-89.02	-67.41
Maritsa	-0.01	1.56	0.32	0.27	-65.12	6.91
Goeksu	-0.49	-83.36	0.26	0.05	-94.07	-66.58
Arno	-0.18	-29.77	0.32	0.13	-84.83	8.13

Kopru	/					
Ebro	0.10	2.86	0.33	0.45	-45.08	4.42

Table S6: Summary of the performances (KGE, bias, correlation, relative standard deviation, low-flow and high-flow biases) of HD model at 5 minutes spatial resolution for each river basin, evaluated over the entire 1990-2014 period.

Basin	KGE	Percent bias	Spearman's rho	Relative SD	High-flow Percent Pbias	Low-flow Percent Pbias
Danube	-0.02	-19.02	0.21	0.30	-45.14	-8.82
Rhone	-0.05	-15.30	0.31	0.22	-64.42	-6.55
Po	-0.01	-29.79	0.53	0.21	-74.04	-21.67
Ceyhan	0.12	-27.36	0.50	0.32	-64.56	-7.97
Adige	0.18	38.65	0.55	0.44	-37.52	16.82
Tiber	-0.07	-52.18	0.60	0.18	-78.90	-59.56
Maritsa	0.31	6.41	0.64	0.40	-50.96	7.33
Goeksu	-0.05	-36.57	0.58	0.17	-80.35	-6.63
Arno	-0.13	-28.15	0.34	0.13	-84.43	9.83
Kopru	-0.22	-68.48	0.64	0.10	-89.17	-61.27
Ebro	-0.05	49.63	0.42	0.33	-53.01	37.40

105 **Table S7: Optimal values of calibrated parameters for each river basin.**

Parameters	Default value	Danube	Rhone	Ceyhan	Adige	Tiber	Goeksu	Arno	Ebro
bexp	1.000	0.480	1.881	0.435	0.424	1.503	0.959	1.848	1.892
smcmax	1.000	1.198	1.198	1.155	1.193	0.816	0.835	1.195	1.199
dksat	1.000	1.029	0.347	0.751	0.368	0.342	1.087	0.579	0.575
rsurfexp	5.000	5.213	4.990	4.869	5.972	3.471	2.369	5.732	5.899
refkdt	1.000	3.722	1.461	3.057	3.987	1.486	3.468	3.796	1.447
slope	0.300	0.013	0.104	0.016	0.026	0.890	0.103	0.010	0.021
retdeprtfac	1.000	5.095	8.763	9.218	3.850	0.142	9.893	0.731	4.848
lksatfac	1000.0	959.3	3700.3	3681.9	836.0	6606.1	6093.3	4633.8	2194.8
ovroughrtfac	1.000	0.919	0.996	0.964	0.993	0.027	0.768	0.922	0.971
zmax	50.00	249.2	247.8	249.7	231.3	249.2	10.76	249.0	63.35

expon	3.000	3.075	1.930	3.339	4.453	3.308	1.082	1.003	1.401
Coeff	0.001	0.046	0.020	0.096	0.099	0.083	0.010	0.002	0.006
cwpvt	1.000	0.548	0.533	0.596	0.513	0.542	1.952	0.760	0.530
vcmx25	1.000	1.004	1.006	0.648	1.368	0.641	1.400	0.816	1.147
mp	1.000	1.095	1.023	0.601	1.376	0.959	1.389	1.281	1.311
hvt	1.000	0.253	0.302	1.342	0.254	0.451	0.364	0.970	0.254

References

Jordan, R. E.: A one-dimensional temperature model for a snow cover: Technical documentation for SNTHERM, 89, https://erdc-library.erdc.dren.mil/jspui/bitstream/11681/11677/1/SR-91-16.pdf (last access: 13 June 2025), 1991.

Niu, G.-Y. and Yang, Z.-L.: Effects of Frozen Soil on Snowmelt Runoff and Soil Water Storage at a Continental Scale, J. Hydrometeorol., 7, 937–952, https://doi.org/10.1175/JHM538.1, 2006.

Verri, G., Pinardi, N., Gochis, D., Tribbia, J., Navarra, A., Coppini, G., and Vukicevic, T.: A meteo-hydrological modelling system for the reconstruction of river runoff: the case of the Ofanto river catchment, Natural Hazards and Earth System Sciences, 17, 1741–1761, https://doi.org/10.5194/nhess-17-1741-2017, 2017.

Yamazaki, D., Kanae, S., Kim, H., and Oki, T.: A physically based description of floodplain inundation dynamics in a global river routing model, Water Resour. Res., 47, https://doi.org/10.1029/2010WR009726, 2011.